AIAA JOURNAL
Vol. 31, No. 1, January 1993

Electron-Ion Three-Body Recombination Coefficient of Argon

T. G. Owano* and C. H. Kruger†
Stanford University, Stanford, California 94305
and
R. A. Beddini‡
University of Illinois, Urbana, Illinois 61801

Spectroscopic measurements of a 15-kW flowing argon plasma, produced by an atmospheric pressure radio frequency inductively coupled plasma torch, have been made. The plasma is found to be in partial local thermodynamic equilibrium at electronic levels as low as $4p$. Ionizational nonequilibrium is observed in the form of an elevated electron density due to the finite three-body electron-ion recombination rate. The flowing plasma is modeled using a two-dimensional axisymmetric flow code, incorporating partial local thermodynamic equilibrium effects, radiative transfer, and ionizational nonequilibrium through the coupled electron continuity equation. Measurement of the inlet and outlet conditions of a controlled test section through which the plasma flows permits an iterative study to attain the electron-ion three-body recombination rate. This rate is found to be higher, in the temperature range considered, than those reported previously in other studies.

Nomenclature

A_{ji} = Einstein A coefficient, s^{-1}
c = speed of light, m/s
c_p = specific heat, J/kg/K
D_a = electron ambipolar diffusion coefficient, m^2/s
e = electron charge, C
f_{12} = oscillator strength
G_f = complex source term
g_i = ion ground state degeneracy
g_j = degeneracy of jth level
h = specific sensible static enthalpy, J/kg
I_b = total black-body function, W/m^2
I_{ji} = emission coefficient, $W/m^3/sr$
$I_{\nu b}$ = spectral black-body function, Ws/m^2
K_{eq} = equilibrium constant, m^{-3}
k = Boltzmann constant, eV/K
k_{fM} = M catalyzed forward rate coefficient, m^3/s
k_{rM} = M catalyzed backward rate coefficient, m^6/s
m_x = mass of particle type x, kg
n = index of refraction
n_j = number density of jth level, m^{-3}
n_x = number density of particle type x, m^{-3}
p = pressure, Pa
p_x = partial pressure of particle type x, Pa
Q_x = partition function of particle type x
Q_{xx} = effective hard sphere cross section for xx, m^2
r = radial coordinate, m
S^*_{aM} = first excitation cross section, m^2/eV
S_r = volumetric radiative source strength, $W/m^3/sr$
S_{12} = line strength, $m^{-1}\ Pa^{-1}\ s^{-1}$
T_B = Boltzmann temperature, K
T_{LTE} = absolute line intensity temperature, K
T_{Saha} = Saha equilibrium temperature, K
T_x = temperature of particle type x, K
U_e = diffusion velocity of electrons, m/s
u = mass velocity of plasma, m/s
u, v, w = axial, radial, and circumferential velocities, respectively, m/s
v_e = radial electron diffusion velocity, m/s
x = axial coordinate, m
α = degree of ionization
α' = electron-catalyzed three-body recombination coefficient, k_{re}, m^6/s
α_j = nonequilibrium factor of level j
α_{ne} = nonequilibrium factor of electrons
β = over-population factor of $4s$ level
β_R = Rosseland mean extinction coefficient, m^{-1}
β_ν = spectral absorption coefficient, m^{-1}
γ = loss factor
δ = thermal conductivity parameter, γ_{tot}/c_p, kg/m/s
ϵ^*_{a1} = energy of first electronic excitation, eV
ϵ_{ion} = ionization energy, eV
ϵ_j = energy of jth electronic level, eV
$\epsilon_{j\lambda}$ = ionization energy of jth level, eV
ϵ_o = permittivity of free space, $C^2/N/m^2$
Θ^*_{a1} = characteristic first excitation temperature, ϵ^*_{a1}/k, K
Θ_{ion} = characteristic ionization temperature, ϵ_{ion}/k, K
λ = wavelength of transition, m
λ_{impact} = impact thermal conductivity, W/m/K
λ_R = reactive thermal conductivity, W/m/K
λ_{rad} = radiative thermal conductivity, W/m/K
λ_{tot} = total thermal conductivity, W/m/K
λ_x = impact thermal conductivity of particle type x, W/m/K
μ = dynamic viscosity, kg/m/s
μ_f = generalized transport coefficient
ν = frequency, s^{-1}
ν_o = line center frequency, s^{-1}
ρ = density, kg/m^3
σ = Boltzmann constant, $W/m^2/K^4$
$\phi(\nu)$ = Voigt line-shape function, s
£ = Rosseland mean free photon length, m

Subscripts

a = atom
aa = atom-atom collision
ae = atom-electron collision
ai = atom-ion collision
e = electron
h = heavy particle
i, ion = ion
M = energetic catalyst

Received Dec. 4, 1991; revision received April 17, 1992; accepted for publication April 17, 1992.

*Research Associate, High Temperature Gasdynamics Laboratory, Department of Mechanical Engineering. Member AIAA.
†Senior Associate Dean, Terman Engineering Center. Member AIAA.
‡Associate Professor, Department of Aeronautical and Astronautical Engineering. Associate Fellow AIAA.

Introduction

An important aspect of understanding and modeling plasma flows is the production and destruction of electron-ion pairs in both equilibrium and nonequilibrium situations. For a recombining plasma of a monatomic gas, there are two important channels through which recombination occurs, namely radiative recombination and three-body collisional recombination. In a highly rarefied plasma where collisions are infrequent, radiative recombination becomes the dominant mode. In denser plasmas, such as the atmospheric pressure plasma studied here, the collision rates are very high, and three-body electron-ion and electron-atom recombination dominate.

Radiative recombination is a negligible contribution to the overall electron-ion recombination rate for the argon plasmas studied here, although it is responsible for the continuum radiation that is used as a spectroscopic measure of the electron density. Electron-ion and electron-atom three-body ionization/recombination are represented by the reversible reactions:

$$Ar^+ + e^- + e^- \Longleftrightarrow Ar + e^- \tag{1}$$

$$Ar^+ + e^- + Ar \Longleftrightarrow Ar + Ar \tag{2}$$

The most widely used argon three-body recombination coefficients are those of Hoffert and Lien,[1] who postulated that the rate-controlling processes are collisional excitation and de-excitation of the first electronically excited state of argon ($\epsilon_2 \approx 11.6$ eV), in the two-step ionization/recombination process:

$$Ar + M \Longleftrightarrow Ar^* + M \tag{3}$$

$$Ar^* + M \Longleftrightarrow Ar^+ + e^- + M \tag{4}$$

representing the overall reaction path:

$$Ar + M \Longleftrightarrow Ar^+ + e^- + M \tag{5}$$

where M is an energetic catalyst (either Ar or e^-) and Ar* is the first electronically excited state of argon. In their work, first excitation cross sections S^*_{aM}, were obtained from Kelly[2] for three-body collisions with neutral species and from Petschek and Byron[3] for collisions with electrons as the third body. The forward rate coefficients for Eq. (5) can then be given as:

$$k_{fM}(T_M) = S^*_{aM}\left[\frac{32}{\pi}\left(\frac{m_s + m_M}{m_a m_M}\right)\right]^{1/2}(kT_M)^{3/2} \times \left(\frac{\Theta^*_{a1}}{2T_M} + 1\right)\exp\left(\frac{-\Theta^*_{a1}}{T_M}\right) \tag{6}$$

The recombination coefficients are then determined using the equilibrium constants for the overall reaction path (5):

$$K_{eq}(T_M) = \frac{2Q_i}{Q_a}\left(\frac{2\pi m_e k T_M}{h^2}\right)^{3/2}\exp\left(\frac{-\Theta_{ion}}{T_M}\right) \tag{7}$$

Inserting the proper values and using the detailed balance relation $k_{rM}(T_M) = k_{fM}(T_M)/K_{eq}(T_M)$ (which is strictly valid only at states of chemical equilibrium, but extensions to nonequilibrium are generally accepted) yields:

$$k_{ra}(T) = 5.80 \times 10^{-37}\left(\frac{\Theta^*_{a1}}{T} + 2\right)\exp\left(\frac{\Theta_{ion} - \Theta^*_{a1}}{T}\right), \quad [\text{cm}^6/\text{s}] \tag{8}$$

$$k_{re}(T_e) = 1.290 \times 10^{-32}\left(\frac{\Theta^*_{a1}}{T_e} + 2\right)\exp\left(\frac{\Theta_{ion} - \Theta^*_{a1}}{T_e}\right), \quad [\text{cm}^6/\text{s}] \tag{9}$$

where for argon $\Theta^*_{a1} = 135{,}300$ K, $\Theta_{ion} = 183{,}100$ K, and $\Theta_{ion} - \Theta^*_{a1} = 47{,}800$ K is the characteristic temperature for single ionization from the first excited state. For the conditions encountered in the argon plasmas studied here, the atom catalyzed three-body recombination only becomes significant at temperatures of approximately 4000 K and below, and so it is neglected. In 1968, Hoffert[4] incorporated more recent cross-section data for the electron catalyzed three-body recombination.[5] This value is approximately 2.85 times the value used in deriving Eq. (9) and yields the rate:

$$\alpha'(T_e) = 3.68 \times 10^{-32}\left(\frac{\Theta^*_{a1}}{T_e} + 2\right)\exp\left(\frac{\Theta_{ion} - \Theta^*_{a1}}{T_e}\right), \quad [\text{cm}^6/\text{s}] \tag{10}$$

where $\alpha' = k_{re}$ is the more commonly used symbol for the three-body recombination rate. It is interesting to note that this paper[4] is almost always overlooked, and that the most widely used three-body recombination rate remains Eq. (9).

In an effort to investigate this important rate coefficient, the spectroscopic investigation of a flowing argon plasma is used as a data base for a computational simulation of the plasma evolution from the entrance of a controlled reactor to its exit. By comparing the measurements to a two-dimensional computational model of the flow and taking into account the various nonequilibrium effects, an estimate of the electron-ion three-body recombination rate can be obtained.

Experimental Facility

The measurements described here were conducted with a nominally 50-kW TAFA model 66 rf induction plasma torch powered by a LEPEL model T-50 power supply. The vertical 5-coil torch has a 7.5-cm inner diameter and an inner length of 26.5 cm measured between the gas-injection plate and the 5-cm exit nozzle, which is 6 cm above the upper coil. The present experiments were conducted downstream of the nozzle using a water cooled quartz test section which is shown schematically in Fig. 1. The test section has an inner diameter of 5 cm and a length of 17.5 cm above the nozzle exit. Spectroscopic measurements reported at the nozzle exit were made 1 cm downstream of the nozzle with the test section removed. To check for the possible effects of air entrainment on the argon plasma, measurements at the same location with the test section in place were made through the single quartz tube below the cooling water passage and yielded the same results as for the unconfined plasma within the 4-cm core for which results are presented here. Similarly, measurements made at the test section exit were made in the freejet 1 cm downstream of the test section exit. The power supply and torch, and the test section cooling water systems, were separately instrumented with thermocouples and flow meters in order to independently obtain calorimetric energy balances for comparison with those obtained from spectroscopic measurements.

Plasma emission measurements were made using a SPEX model 1400-11 ¾-m scanning monochromator fitted with a Hamamatsu model R928 photomultiplier tube. Absolute intensity calibrations were obtained by means of a tungsten strip lamp, with a calibration traceable to National Bureau of Standards standards. Temperature measurement of the tungsten

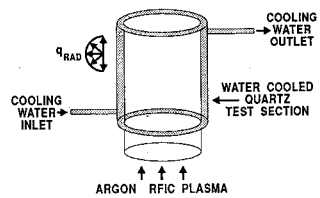

Fig. 1 Schematic of water cooled test section.

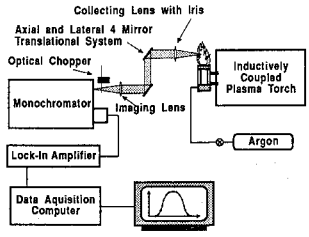

Fig. 2 Schematic of emission measurements.

strip lamp was made using a Pyro-micro disappearing filament optical pyrometer and is the principal source of uncertainty in the intensity calibration (~5%). Ultraviolet calibration was obtained using a calibrated quartz-halogen, type FEL, tungsten coiled-coil filament lamp. The four-mirror optical arrangement, which permitted lateral and axial scanning of the plasma, is shown qualitatively in Fig. 2. Data sets acquired using a Stanford Research Systems model SR510 lock-in amplifier were transferred and stored on a laboratory computer for processing. Lateral traverses of emission data were transformed to radial variations within the plasma using an Abel inversion technique.[6]

Temperature Measurements

Several approaches have been used for temperature determination in thermal plasmas, including measurement of absolute line intensities, comparison of relative line intensities, and interpretation of continuum intensities from recombination by use of the Saha equation.[7] If, and only if, the plasma is in local thermodynamic equilibrium (LTE), these techniques will be equivalent, in principle, but with differing sensitivities and accuracy. On the other hand, departures from LTE could produce unknown errors in the inferred temperature. Such errors would occur, for example, if recombination radiation were used to infer the temperature under circumstances where the electron density is not in Saha equilibrium with the ground-level density. In the present measurements, radial distributions of the absolute and relative intensities of eight lines of neutral argon along with the absolute recombination radiation at 533 nm were measured and independently interpreted to assess the significance of departures from LTE.

A typical Boltzmann plot of relative line intensities is shown in Fig. 3 for a torch plate power of 46.7 kW and an argon flowrate of 160 slpm (0.00443 kg/s). Spectroscopic data for the measured argon lines is given in Ref. 8. The temperatures derived from these Boltzmann plots are determined using a weighted least-squares linear fit, where the weighting is determined from the experimental uncertainty in the measured line intensity, incorporating both measurement and calibration uncertainties, uncertainties introduced in the Abel inversion of the lateral data, and the reported uncertainty in the Einstein coefficients. Boltzmann temperatures T_B calculated from the slope of Boltzmann plots such as Fig. 3 are compared with temperatures based on the absolute intensity of the ArI line at 430 nm in Figs. 4 and 5 for the torch nozzle exit and test section exit, respectively. Torch conditions for these figures are the same as in Fig. 3.

Here the absolute line intensity temperatures are denoted by T_{LTE} and are calculated from the Maxwell-Boltzmann relation:

$$\frac{n_j}{g_j} = \left(\frac{1}{g_j}\right)\left(\frac{1}{kT_{\mathrm{LTE}j}}\right)\exp\left(\frac{-\epsilon_j}{kT_{\mathrm{LTE}j}}\right) \tag{11}$$

To obtain an absolute number density from a measured emission coefficient I_{ij} [W/cm^{3}sr], the following relation is used

$$n_j = \frac{4\pi I_{ji}\lambda}{hcA_{ji}} \tag{12}$$

where I_{ji} is determined from the recorded photomultiplier tube signal through the aforementioned tungsten lamp calibration. For convenience and clarity, in Eq. (11), p/kT has been substituted for the ground level density n_1; this follows from the fact that, for all experimental conditions reported here, the electron number density is small compared to the total argon number density, and the electronic partition function is essentially the ground-level degeneracy g_1. Although Figs. 4 and 5 show T_{LTE} based on just the 430 nm ArI line, numerical values for T_{LTE} when based on other lines with relatively well-known Einstein coefficients agree within 1%.

Electron Density Measurements

One can also use the absolute continuum intensity to determine the electron density. The absolute continuum emissivity of the plasma due to electron-ion free-free interaction, electron-atom free-free interaction, and electron-ion free-bound interaction[7] is strongly dependent on the electron density and weakly dependent on the electron temperature at wavelengths greater than about 400 nm. Thus, the absolute electron number density can be calculated from the absolute emission coefficient of the continuum radiation measured at 533 nm, using T_B in the weak temperature dependence. (Here, the electron-ion free-bound Biberman factor used at 533 nm was 1.7, and the relative contributions of the electron-ion free-bound, electron-atom free-free, and electron-ion free-free interactions are of the order of 25:5:1, respectively.) The results of this reduction are shown in Fig. 6 for the nozzle and test section exits. It is important to note that the interpretation of the absolute continuum radiation to determine electron density does not rely on any assumptions of equilibrium between the free electrons and the ground state. Because of this fact, the technique yields accurate electron densities for plasmas in LTE as well as for those in partial local thermodynamic equilibrium (PLTE).

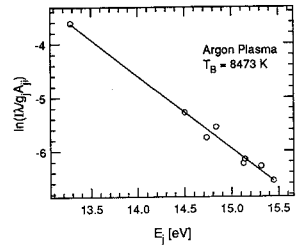

Fig. 3 Typical Boltzmann plot.

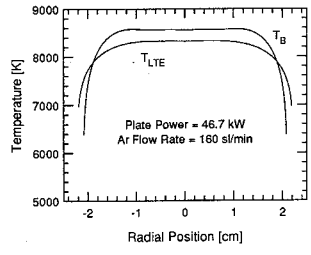

Fig. 4 Comparison of T_B with T_{LTE} at the nozzle exit.

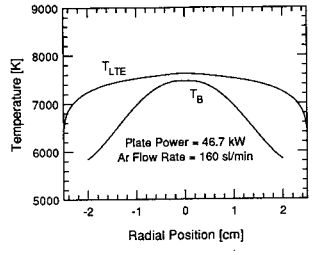

Fig. 5 Comparison of T_B with T_{LTE} at the test section exit.

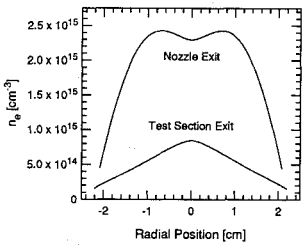

Fig. 6 Electron densities calculated from measured absolute continuum intensities.

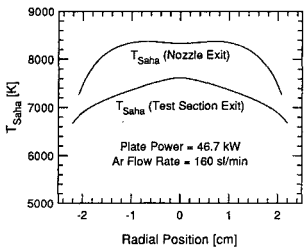

Fig. 7 Saha temperatures inferred from measured electron densities.

It is useful, however, once one has determined the electron density, to consider at what equilibrium temperature this electron density would exist. One can determine this Saha equilibrium temperature T_{Saha} through the use of the ground state Saha equation:

$$\frac{n_e n_i}{n_a} = 2\left(\frac{Q_i}{Q_a}\right)\left(\frac{2\pi m_e k T_{\text{Saha}}}{h^2}\right)^{3/2} \exp\left(\frac{-\epsilon_{\text{ion}}}{kT_{\text{Saha}}}\right) \tag{13}$$

where the ground state number density n_a can be replaced by p/kT, Q_a can be replaced by the ground state degeneracy, and similarly Q_i, the ion partition function, can be replaced by the ion ground state degeneracy. The results of these calculations for the nozzle and test section exits are plotted in Fig. 7 and show that the Saha equilibrium temperature T_{Saha} is much closer to the absolute line intensity temperature T_{LTE} than to the Boltzmann relative intensity temperature T_B. The fact that T_{Saha} is closer in value to T_{LTE} than to T_B is not surprising since, in contrast to T_B, the determination of T_{Saha} and T_{LTE} requires knowledge of the ground state number density; thus both procedures entail the same assumption of equilibrium between the ground and excited states.

Partial Equilibrium Model

These results show that for the nozzle exit, in the central region of the plasma, the Boltzmann temperature T_B is approximately 250 K above T_{LTE}. This difference is consistent with depopulation of bound electronic states, although it is within the ~5% uncertainty of the temperature measurements. On the other hand, at both the nozzle and the test section exits (Figs. 4 and 5), T_{LTE} is greater than T_B in the outer regions of the plasma, which is consistent with both diffusion of free electrons toward the cool walls and with the finite electron recombination rates[9] controlling the decay from the initially high electron densities generated within the rf discharge region. Although this nonequilibrium is small at the nozzle exit, it is pronounced for the recombining plasma at the test section exit.

A detailed review of all of the data shows that they can be interpreted in terms of a partial equilibrium model in which the bound and free electrons are mutually in partial equilibrium at the Boltzmann temperature T_B, as given by the excited state Saha equation:

$$\frac{n_e^2}{n_j} = 2\left(\frac{g_i}{g_j}\right)\left(\frac{2\pi m_e k T_B}{h^2}\right)^{3/2} \exp\left(\frac{-\epsilon_{j\lambda}}{kT_B}\right), \qquad j>2 \tag{14}$$

An argon collisional-radiative model[10] indicates that the population of the first excited level ($j=2$) will begin to deviate from equilibrium with the free electrons at sufficiently low ($<10^{15}$ cm^{-3}) electron densities and begin to move toward equilibrium with the ground level ($j=1$). Thus, the partial equilibrium model is defined by Eq. (14), with $j>2$. (With strong $4p$-$4s$ radiative loss, the partial equilibrium may not exist until $j>3$ (Ref. 11); however, this is not anticipated until electron densities fall below 10^{14} cm^{-3} and to the accuracy of our measurements, we did not observe such an effect.)

Since the partial equilibrium described by this model is maintained by collisions between excited electronic states and free electrons, the Boltzmann temperature T_B should agree with the free electron translational temperature T_e. This is supported by detailed collisional-radiative calculations[10-13] that show equilibration, at sufficiently high electron densities, between the electron temperature T_e and the Boltzmann slope temperature T_B of high-lying bound electronic states. In the absence of plasma currents in the region under study, the electron energy equation[9] shows relatively small differences ($\approx 1\%$) between the electron temperature T_e and the heavy particle gas temperature T_h for the conditions of our experiments, except near the test section wall where steep T_e gradients exist.

The partial equilibrium model thus allows the plasma to be described by three parameters: the pressure, the temperature T_B, and a nonequilibrium factor. This factor α is defined by:

$$\frac{n_j}{g_j} = \alpha_j\left(\frac{1}{g_1}\right)\left(\frac{p}{kT_B}\right)\exp\left(\frac{-\epsilon_j}{kT_B}\right) \tag{15}$$

$$\frac{n_e^2}{p/kT_B} = \alpha_{\text{ne}}\left(\frac{2g_i}{g_1}\right)\left(\frac{2\pi m_e k T_B}{h^2}\right)^{3/2} \exp\left(\frac{-\epsilon_{\text{ion}}}{kT_B}\right) \tag{16}$$

A property of the partial equilibrium model is that α_j and α_{ne} are the same, and that α_j is independent of j, for $j>2$.

Computational Model

To extract an accurate estimate of the electron-ion three-body recombination rate from the knowledge of the plasma state at the entrance and exit of the plasma flow reactor requires more than a simple stream tube type analysis. Although knowledge of the electron density at two points and an estimate of the flow time in between yields an electron destruction rate, the complete effects of geometry, finite rate reactions, convection, diffusion, thermal conductivity, and radiative transfer can only be accounted for by a full simulation of the plasma flowfield. For these reasons, an axisymmetric, two-dimensional, parabolized Navier-Stokes plasma code[14] was used as a base to create a nonequilibrium, finite rate electron chemistry, plasma flow simulation. This model incorporates accurate thermophysical properties of argon into the solution, as well as a nonequilibrium radiative heat flux (from the optically thin plasma radiation), optically thick radiation transport through an effective radiative thermal conductivity, nonequilibrium electron thermal conductivity, and a coupled solution of the electron continuity equation.

Accurate prediction of the radiative transport is essential to energy loss and transport mechanisms, and the effects of partial local thermodynamic equilibrium must be taken into account. Use of the experimentally determined volumetric radiative loss[8] is made to incorporate the effects of nonequilibrium radiative transfer. In this case, since the effects of finite rate electron-ion recombination cause an elevated electron density (and thus elevated excited electronic level populations), the net effect is to cause a higher radiative loss than would be expected under equilibrium conditions. Another effect of this elevated electron population is to increase the component of thermal conductivity due to electrons, which at plasma temperatures can be significant if not dominant. A nonequilibrium form of the electron continuity equation is

coupled to the flowfield solution and predicts the convection, diffusion, and destruction of electron-ion pairs as the flow progresses through the test section.

Basic Model

The plasma flow code used as a starting point for building a complete nonequilibrium plasma simulation is a parabolic approximation for the Navier-Stokes equations utilizing a second-order turbulence model for Reynolds stresses and energy correlations.[14] Although this program is capable of handling a turbulent or transition flow, the argon plasma considered here has a Reynolds number of approximately 2×10^2 and is basically a laminar flow, with the turbulence equations solved but having negligible impact on the solution. The parabolic equation system is comprised of the nonconservative forms of the axial velocity and sensible static enthalpy equations used by Beddini.[15] The mass continuity, axial momentum, energy, and second-order turbulence model equations for Reynolds stresses and energy correlations are also adapted from Ref. 15.

The parabolic differential equation system for the fluid may be considered in the functional form:

$$\overline{\rho u}\frac{\partial f}{\partial x}+\overline{\rho v}+\frac{\partial f}{\partial r}=\frac{1}{r^{\nu}}\frac{\partial}{\partial r}\left(r^{\nu}\overline{\mu_f}\frac{\partial f}{\partial r}\right)+G_f(f) \tag{17}$$

where

$$f=\left\{\bar{u},\bar{h},\overline{u'u'},\overline{v'v'},\overline{w'w'},\overline{u'v'},\overline{h'u'},\overline{h'v'},\overline{h'h'},\right\}^T \tag{18}$$

The transport coefficient μ_f represents the dynamic viscosity μ or the thermal conductivity parameter δ as appropriate for each equation. However, not all of the diffusion terms for each equation in the system may be cast in the form shown in Eq. (17). Those that do not conform are implicitly contained within the complex function G_f, which also represents the sources, cross-coupling, and dissipation terms for the equations. For the mean enthalpy equation, the volumetric radiative loss S_r is also included within G_f.

The numerical solution procedure for the differential equation system utilizes an implicit Crank-Nicholson method. Block decoupling of the 11 dependent variables is used to accelerate the solution using the tridiagonal algorithm. The largest sub-block size solved is 3×3. An unequally spaced, dynamically adaptive grid is employed in both the axial and radial directions. The radial mesh is varied inversely with the curvature of selected dependent variables, allowing effective resolution of regions of rapid change of the mean flow, energy, and Reynolds stresses. To complete the solution procedure, v is found by quadrature of the continuity equation, and the axial pressure gradient is determined iteratively by satisfaction of global mass continuity over an axial step.

Electron Continuity Equation

The heart of this investigation into the electron-ion three-body recombination rate for argon is the electron continuity equation. It controls the convection, diffusion, and destruction of electron-ion pairs as the plasma flows down the test section. The electron continuity equation in its most general form[16] is given by

$$\frac{\partial n_e}{\partial t}+\nabla\cdot[n_e(u+U_e)]=\dot{n}_e \tag{19}$$

For the two-dimensional axisymmetric plasma under consideration,

$$u=\{u,v\} \tag{20a}$$

$$U_e=v_e \tag{20b}$$

$$\frac{\partial n_e}{\partial t}=0 \tag{20c}$$

thus,

$$\frac{1}{r}\frac{\partial}{\partial r}[rn_e(v+v_e)]+\frac{\partial}{\partial z}(n_eu)=\dot{n}_e \tag{21}$$

For the ambipolar diffusion of electrons we can write

$$n_ev_e=\frac{-D_a}{2kT}\frac{\partial}{\partial r}(p_e+p_i) \tag{22}$$

where D_a is taken from Devoto.[17] For this singly ionized plasma,

$$p_e=p_i=n_ekT \tag{23}$$

The right-hand side of Eq. (15) represents the production/destruction of electron-ion pairs and contains the recombination rate under investigation. This source term, for a plasma in LTE or PLTE, is given by the equation[9]:

$$\dot{n}_e=\alpha' n_e\left[n_1\left(\frac{n_e^2}{n_1}\right)^*-n_e^2\right] \tag{24}$$

where

$$\left(\frac{n_e^2}{n_1}\right)^*=2\left(\frac{g_i}{g_1}\right)\left(\frac{2\pi m_ekT_h}{h^2}\right)^{3/2}\exp\left(\frac{-\epsilon_{\text{ion}}}{kT_h}\right) \tag{25}$$

is the Saha equation for electron density in LTE at the heavy particle temperature T_h. Although investigation indicates that the flowing argon plasma is in a state of PLTE extending down to the second excited electronic level ($4p$), the first excited level ($4s$) may or may not be in PLTE with the free electrons. This is of importance here because the rate limiting step for the electron-ion three-body recombination process involves this level. The deviation of the first excited level from PLTE with the free electrons can be written as:

$$\left(\frac{n_2}{n_e^2}\right)=\beta\left(\frac{n_2}{n_e^2}\right)^{\text{PLTE}} \tag{26}$$

where β is the overpopulation of the $4s$ level with respect to the PLTE distribution of excited states and free electrons. The effect of this overpopulation factor is to modify Eq. (24) to the form:

$$\dot{n}_e=\alpha' n_e\left[\frac{n_1}{\beta}\left(\frac{n_e^2}{n_1}\right)^*-n_e^2\right] \tag{27}$$

To determine this overpopulation factor β, we make use of a recently developed 23-level collisional-radiative model for argon[10] and consider the limiting case of a stationary state plasma. In a stationary state, we can solve the source term as:

$$\dot{n}_e=0=\alpha' n_e\left[\frac{n_1}{\beta}\left(\frac{n_e^2}{n_1}\right)^*-\frac{n_e^2}{\gamma}\right]^{\text{stationary state}} \tag{28}$$

thus,

$$\left(\frac{n_e^2}{n_1}\right)^{\text{stationary state}}=\left(\frac{\gamma}{\beta}\right)\left(\frac{n_e^2}{n_1}\right)^* \tag{29}$$

where we have added an additional factor γ to accommodate other small, unaccounted for loss mechanisms (such as depopulation of excited states due to radiation loss). By using the complete collisional radiative model to predict steady-state population densities, Eqs. (26) and (29) can be solved for the quantities β and γ as a function of electron density. The results of these calculations are shown in Figs. 8 and 9 for the electron density range encountered in the argon plasma under study. The complete electron continuity equation used for this simulation thus becomes

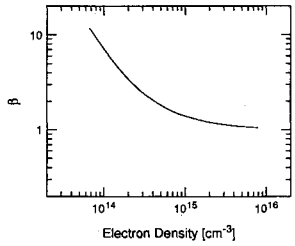

Fig. 8 Overpopulation factor for the 4s level with respect to PLTE.

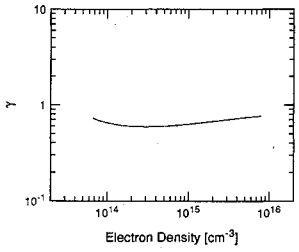

Fig. 9 Loss factor for the electron source term.

$$\frac{1}{r}\frac{\partial}{\partial r}(rn_e v)-\frac{1}{r}\frac{\partial}{\partial r}\left[\frac{rD_a}{kT}\frac{\partial}{\partial r}(n_e kT)\right]+\frac{\partial}{\partial z}(n_e u)$$

$$=\alpha' n_e\left[\frac{n_1}{\beta}\left(\frac{n_e^2}{n_1}\right)^*-\frac{n_e^2}{\gamma}\right] \tag{30}$$

along with Eq. (25).

Nonequilibrium Effects

Since the argon plasma is in a state of PLTE instead of LTE, certain properties of the plasma will differ significantly from their LTE values. These properties include the thermal conductivity, the plasma optically thin radiation, and the plasma optically thick radiation. Other properties such as the specific heat and viscosity are not significantly affected.

Thermal Conductivity

The coefficient of thermal conductivity for a monatomic plasma has contributions from impact, reactive, and radiative thermal conductivities. The impact thermal conductivities are due to the action of atoms, electrons, and ions. Fay and Kemp[18] propose a mixture rule formula for the impact thermal conductivity:

$$\lambda_{\text{impact}}=\lambda_s\left(1+\sqrt{2}\frac{m_e}{m_a}\frac{\lambda_s}{\lambda_a}\frac{Q_{ae}}{Q_{aa}}\frac{1-\alpha}{\alpha}\right)^{-1}$$

$$+\lambda_a\left(1+\frac{Q_{ai}}{Q_{aa}}\frac{\alpha}{1-\alpha}\right)^{-1} \tag{31}$$

where

$$\lambda_a=2.4\times10^{-6}T_h^{3/4}\left[\frac{\text{W}}{\text{cm K}}\right] \tag{32}$$

$$\lambda_s=\frac{1.84\times10^{-12}T_e^{5/2}}{\frac{1}{4}\ell n(\Lambda_1^4+\Lambda_2^4+e^4}\left[\frac{\text{W}}{\text{cm K}}\right] \tag{33}$$

$$\Lambda_1=1.24\times10^4\left(\frac{T_e^{3/2}}{\sqrt{n_e}}\right) \tag{34}$$

$$\Lambda_2=1800\left(\frac{T_e}{\sqrt[3]{n_e}}\right) \tag{35}$$

$$\frac{Q_{ae}}{Q_{aa}}=1.5\times10^{-2},\qquad \frac{Q_{ai}}{Q_{aa}}=1.44T_h^{0.16} \tag{36}$$

$$\lambda_e=\lambda_i\left(\frac{m_i}{m_e}\right)^{1/2}=(1+\sqrt{2})\lambda_s \tag{37}$$

Although it is difficult to readily discern the dependence of λ_{impact} on the electron density, it is quite significant for even small ionization fractions. For this reason, the full form of the impact thermal conductivity (31) is retained to accurately account for the electron density overpopulation in this recombining PLTE plasma.

The reactive thermal conductivity is that contribution arising from the diffusion of electron-ion pairs, which carry potential energy of an amount equal to the ionization energy, from one region to another. Using the formulation of Devoto[17] and neglecting the small ($\approx 1\%$) contribution from thermal diffusion we can write:

$$\lambda_R=\frac{n_e\epsilon_{\text{ion}}^2}{2kT^2}\frac{1}{[1-2(n_e/n)]}\frac{1}{(1+n_e/n_a)}D_a \tag{38}$$

where $n=p/kT$ is the total gas density. For the small ionization fractions of the plasmas under study, the reactive thermal conductivity is approximately proportional to the electron density and is thus sensitive to the effects of PLTE.

The radiative thermal conductivity is due to the short-range, optically thick, radiative transport occurring within a plasma. This concept arises from the reduction of the equation of radiative transport for the optically thick limit, which results in a diffusion-type equation,[19] where

$$\lambda_{\text{rad}}\equiv\frac{16n^2\sigma T^3}{3\beta_R} \tag{39}$$

$$\frac{1}{\beta_R}\equiv\int_{\nu=0}^{\infty}\frac{1}{\beta_\nu}\frac{\text{d}I_\nu b(T)}{\text{d}I_b(T)}\,\text{d}\nu \tag{40}$$

The majority of the optically thick radiation in argon comes from the resonance transitions between the 4s and ground states. Since this recombining plasma has elevated excited state densities, as well as an elevated 4s population with respect to these already overpopulated excited states, this nonequilibrium contribution to the thermal conductivity can be important. This will be discussed further in the context of optically thick radiation transport. The total thermal conductivity used for this simulation is thus given by

$$\lambda_{\text{tot}}=\lambda_{\text{impact}}+\lambda_R+\lambda_{\text{rad}} \tag{41}$$

where λ_{impact}, λ_R, and λ_{rad} are given by Eqs. (31), (38), and (39), respectively.

Optically Thin Radiation

The optically thin radiative losses of the argon plasma are given by the volumetric radiative loss term[8] S_r. A suitable curve fit for the equilibrium radiation source strength is given by

$$S_r^{\text{eq}}=1.065\times10^{14}\exp\left(\frac{-141{,}170}{T_{\text{LTE}}}\right)\left[\frac{\text{W}}{\text{m}^3}\right] \tag{42}$$

Since the plasma is in PLTE, the actual local radiation will be higher or lower than the equilibrium value by the nonequilibrium factor α.[8] The nonequilibrium optically thin radiation loss can thus be written as

$$S_r=1.065\times10^{14}\,\alpha\exp\left(\frac{-141{,}170}{T_h}\right)\left[\frac{\text{W}}{\text{m}^3}\right] \tag{43}$$

or equivalently as

$$S_r=1.065\times10^{14}\exp\left(\frac{-141{,}170}{T_{\text{Saha}}}\right)\left[\frac{\text{W}}{\text{m}^3}\right] \tag{44}$$

where T_{Saha} is given by Eq. (13).

Optically Thick Radiation

As discussed earlier, the optically thick plasma radiation is treated in the diffusion approximation as radiative thermal conductivity as defined by Eqs. (39) and (40). In a formal analysis of Eq. (40), the spectral and total black-body functions can be substituted, and the approximation of strong absorption only in a narrow region near a resonance line can be applied to yield the equation

$$\frac{1}{\beta_R} \approx \frac{h^2 \pi \nu_o^4}{2c^2 kT^5 \sigma \exp(h\nu_o/kT)} \int_{\nu=0}^{\infty} \frac{1}{\beta_\nu} \, d\nu \tag{45}$$

where

$$\beta_\nu = S_{12} \phi(\nu) p \tag{46}$$

$$S_{12} = \frac{\pi e^2}{4\pi \epsilon_o m_e c p} \left(\frac{n_1}{n}\right) n_1 f_{12} \left[1 - \exp\left(\frac{-h\nu_o}{kT}\right)\right] \tag{47}$$

Here, $\phi(\nu)$ is the Voigt line-shape function incorporating Stark, resonance, and Doppler broadening. For proper evaluation of the integral in Eq. (45), the integration limits are reduced to those frequencies for which the line is optically thick. These limits are thus determined by the physical extent of the plasma (since an infinitely large plasma is optically thick to all frequencies, and an infinitely small plasma is optically thin to all frequencies). It is in the evaluation of these limits that the formal evaluation of the radiative thermal conductivity becomes difficult. Since the plasma is not uniform (and it is this that drives the optically thick radiative transport), the evaluation of these limits based on strictly local properties becomes inaccurate. Radiation excluded from the integration as being optically thin based on local limits may indeed be absorbed in a nearby region whose properties are different. Because of this difficulty, an effective radiative thermal conductivity[20] is often empirically defined as $\lambda_{rad} \propto C\pounds T^3$, where C is an empirical constant. Using information gained from the formal analysis (basically, that £ scales as $\sim T^2$ for the range of conditions encountered), a suitable empirical value for the radiative thermal conductivity was found to be

$$\lambda_{rad} = 1.90 \times 10^{-21} T^5 \left[\frac{\mathrm{W}}{\mathrm{mk}}\right] \tag{48}$$

The magnitude of this radiative thermal conductivity is only $\approx 15\%$ of the impact thermal conductivity at the maximum temperature considered in the plasma flow (≈ 8500 K), but is necessary to accurately predict the evolution of the temperature field.

Results

Using the measured nozzle exit conditions (Figs. 4 and 6) as input to the flow code, the evolution of the plasma flowfield to the test section exit was computed. By iteratively comparing the predicted electron density profile at the test section exit to that measured from the continuum radiation (Fig. 6), the electron-ion three-body recombination rate was adjusted to provide best agreement between the measured and simulated densities in the core region ($r \leq 1.5$ cm). It should also be noted that the related cross section in the collisional-radiative

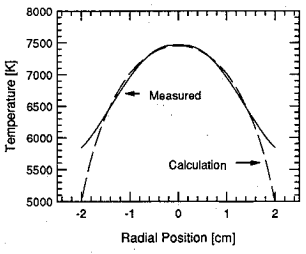

Fig. 10 Comparison of measured and predicted temperature profiles.

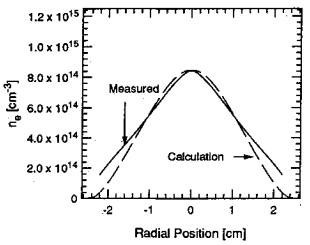

Fig. 11 Comparison of measured and predicted electron density profiles.

model was similarly adjusted to be consistent in the analysis. Since the core flow of the argon plasma covers a relatively small range in temperature as the plasma cools in the test section, the form of the recombination rate [Eq. (10)] was maintained, and only the pre-exponential constant was adjusted. The best fit rate was found be

$$\alpha'(T_e) = 3.30 \times 10^{-32} \left(\frac{\Theta_{a1}^*}{T_e} + 2\right) \exp\left(\frac{\Theta_{\mathrm{ion}} - \Theta_{a1}^*}{T_e}\right), \quad [\mathrm{cm}^6/\mathrm{s}] \tag{49}$$

A 10% variation in this best fit rate causes an approximately 3.5% variation in the predicted electron density (which corresponds to the measurement uncertainty). The comparison of the measured and predicted temperature and electron density profiles are shown in Figs. 10 and 11, respectively. It is very interesting to note that this value of the electron-ion three-body recombination rate is very close to that given by Hoffert,[4] approximately 10% lower, and is approximately 2.5 times the widely used rate of Eq. (9). Although the uncertainties involved in the computational simulation of this flowing nonequilibrium plasma certainly prevent this from being considered an absolute measurement of the electron-ion three-body recombination coefficient, the results here indicate that the rate may be significantly higher than that which is presently in use.

Conclusions

Spectroscopic measurements of a flowing, atmospheric pressure argon plasma have been performed at the inlet and outlet of a controlled test section to ascertain temperatures and electron densities. The plasma is found to be in a state of partial local thermodynamic equilibrium. An axisymmetric, two-dimensional, partial equilibrium flow code with a fully coupled electron continuity equation has been developed to model this nonequilibrium flowfield. Iterative comparison between the experimental and computational flowfield development permitted determination of the dominant electron-ion three-body recombination rate. This rate is found to be approximately equal to a previously reported rate, but approximately two and one-half times larger than the most widely used rate.

Acknowledgments

This research was supported by U.S. Department of Energy Grant DOE-DE-FG03-88ER-13957 and by Air Force Office of Scientific Research Grants AFOSR 86-0225 and 89-0308.

References

[1]Hoffert, M. I., and Lien, H., "Quasi-One-Dimensional, Nonequilibrium Gas Dynamics of Partially Ionized Two-Temperature Argon," *Physics of Fluids*, Vol. 10, No. 8, 1967, pp. 1769–1777.

[2]Kelly, A. J., "Atom-Atom Ionization Cross Sections of the Noble Gases—Argon, Krypton, and Xenon," *Journal of Chemical Physics*, Vol. 45, No. 5, 1966, pp. 1723–1732.

[3]Petschek, H., and Byron, S., "Approach to Equilibrium Ionization behind Strong Shock Waves in Argon," *Annals of Physics*, Vol. 1, No. 3, 1957, pp. 270–315.

[4]Hoffert, M. I., "Precursor Ionization Effects on Magnetohydro-

dynamic Switch-On Shock Structure," *Journal of Plasma Physics,* Vol. 4, Pt. 3, 1970, pp. 477–494.

[5]Zel'dovich, Y. B., and Raizer, Y. P., "Rates of Relaxation Processes in Gases," *Physics of Shock Waves and High Temperature Hydrodynamic Phenomena,* Vol. I, Academic, New York, 1964, pp. 382–440.

[6]Cremers, C. J., and Birkebak, R. C., "Application of the Abel Integral Equation to Spectrographic Data," *Applied Optics,* Vol. 5, No. 6, 1966, pp. 1057–1064.

[7]Wilbers, A. T. M., Kroesen, G. M. W., Timmermans, C. J., and Schram, D. C., "The Continuum Emission of an Arc Plasma," *Journal of Quantitative Spectroscopy and Radiative Transfer,* Vol. 45, No. 1, 1991, pp. 1–10.

[8]Owano, T. G., Gordon, M. H., and Kruger, C. H., "Measurements of the Radiation Source Strength in Argon at Temperatures between 5000 K and 10,000 K," *Physics of Fluids B: Plasma Physics,* Vol. 2, No. 12, 1990, pp. 3184–3190.

[9]Kruger, C. H., "Nonequilibrium in Confined-Arc Plasmas," *Physics of Fluids,* Vol. 13, No. 7, 1970, pp. 1737–1746.

[10]Repetti, T. E., Fincke, J. R., and Neuman, W. A., "Relaxation Kinetics of Argon in Thermal Plasmas," *ASME Heat Transfer in Thermal Plasma Processing,* Vol. 161, No. 1, 1991, pp. 167–175.

[11]Hernberg, R., and Vattulainen, J., "Experimental Study of LTE in a Large RF Argon Plasma," *Proceedings of the 9th International Symposium on Plasma Chemistry,* International Union of Pure and Applied Chemistry, Pugnochiuso, Italy, 1989, pp. 308–313.

[12]Shaw, J. F., Mitchner, M., and Kruger, C. H., "Effects of Nonelastic Collisions in Partially Ionized Gases," *Physics of Fluids,* Vol. 13, No. 2, 1970, pp. 325–345.

[13]Van Der Sijde, B., Van Der Mullen, J. A. M., and Schram, D. C., "Collisional Radiative Models in Plasmas," *Beitrage Aus Der Plasmaphysik,* Vol. 24, No. 5, 1984, pp. 447–473.

[14]Owano, T. G., "Analysis of Turbulent Convective and Radiative Heat Transfer in the Presence of Intense Optical Fields," M.S. Thesis, Univ. of Illinois, Urbana-Champaign, IL, Aug. 1987.

[15]Beddini, R.A., "Injection-Induced Flows in Porous-Walled Ducts," *AIAA Journal,* Vol. 24, No. 11, 1986, pp. 1766–1773.

[16]Mitchner, M., and Kruger, C. H., "Ionizational Nonequilibrium," *Partially Ionized Gases,* Wiley, New York, 1973, pp. 431–493.

[17]Devoto, R.S., "Transport Coefficients of Partially Ionized Argon," *Physics of Fluids,* Vol. 10, No. 2, 1967, pp. 354–364.

[18]Fay, J.A., and Kemp, N.H., "Theory of Heat Transfer to a Shock-Tube End-Wall from an Ionized Monatomic Gas," *Journal of Fluid Mechanics,* Vol. 21, Pt. 4, 1965, pp. 659–672.

[19]Özisik, M.N., "Approximate Methods in the Solution of the Equation of Radiative Transfer," *Radiative Transfer and Interactions with Conduction and Convection,* Wiley, New York, 1973, pp. 313–348.

[20]Dresvin, S.V., "Radiation and Spectral Diagnostics of Low Temperature Plasmas," *Physics and Technology of Low-Temperature Plasmas,* Iowa State Univ. Press, Ames, IA, 1977, pp. 49–140.